Sustainable Energy, Grids and Networks 40 (2024) 101561

Contents lists available at ScienceDirect

Sustainable Energy, Grids and Networks

journal homepage: www.elsevier.com/locate/segan

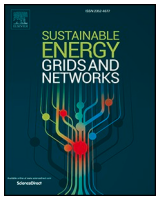

A two-stage online inertia estimation: Identification of primary frequency control parameters and regression-based inertia tracking

Juan Diego Rios-Peñaloza [a,*], Andrea Prevedi [b], Fabio Napolitano [b], Fabio Tossani [b], Alberto Borghetti [b], Milan Prodanovic [a]

[a] Electrical Systems Unit, IMDEA Energy, Madrid, Spain
[b] Dept. of Electrical, Electronic and Information Engineering, University of Bologna, Italy

ARTICLE INFO

Keywords:
Converter-interfaced sources
Effective inertia
Inertia estimation
Parameter identification
Primary frequency control
Regression model

ABSTRACT

In recent years, power system inertia has significantly decreased and has become more variable due to the massive integration of converter-interfaced renewable energy sources. Real-time awareness of the inertia present in the system is essential for operators to take preventive actions and mitigate potential instability risks. Online inertia tracking methods based on field data have been used to accomplish this task. However, most existing methods are disturbance-based and few have proven effective under normal operating conditions. In addition, some methods require prior knowledge of the primary frequency control dynamics, which are usually unknown, especially in presence of power converters. To overcome these limitations, this paper proposes a two-stage online inertia estimation method. The first stage estimates the primary frequency control parameters. The second stage uses a regression-based approach to track the inertia in real time. A sensitivity analysis of the parameters of the regression model is used to determine the conditions under which the primary frequency control parameters must be updated. The performance of the method is validated using the IEEE 39-bus benchmark network under normal operating conditions and under the occurrence of large disturbances. The algorithm is also tested in the presence of converter-interfaced sources controlled in both grid-following and grid-forming modes. Real-time tests validate the applicability of the method.

1. Introduction

1.1. Motivation

The last decade has seen a significant increase in the deployment of renewable energy sources and energy storage systems, most of which are connected to the grid through power electronic converters [1]. As the number of these converter-interfaced sources (CISs) increases, the overall system inertia decreases, affecting the stability of the power system. To mitigate these effects, the use of storage systems controlled to provide virtual inertia has been proposed [2,3], usually mimicking the behaviour of synchronous generators. As a consequence, inertia has become a parameter strongly dependent on the number of CISs connected to the system and the characteristics of their controllers.

In this context, the effective inertia estimation becomes a critical issue. The main aspects are the following.

- The inertia is no longer solely dependent on a physical parameter as in conventional generation but can also depend on the characteristics of the power converters. It depends on the converter control mode (e.g., grid-following, grid-forming), the implemented strategy (e.g., droop control, virtual synchronous machine), and the control parameters [4].
- The amount of inertia in the system varies significantly over time due to the variability of the CISs connected to the system. The unpredictability of renewable energy increases the impact of this variability.
- System operators can use the information on the effective inertia trend to take preventive measures to increase the stability and resilience of the system. Such measures may include the use of synchronous condensers or increasing frequency regulation reserves.
- In addition, system operators themselves may require power plants to provide certain levels of inertia to ensure stability margins, even if they are inverter-based [5]. Inertia estimation algorithms can help to verify the compliance with such requirements.

* Corresponding author.
E-mail addresses: juan.rios@imdea.org (J.D. Rios-Peñaloza), andrea.prevedi2@unibo.it (A. Prevedi), fabio.napolitano@unibo.it (F. Napolitano), fabio.tossani@unibo.it (F. Tossani), alberto.borghetti@unibo.it (A. Borghetti), milan.prodanovic@imdea.org (M. Prodanovic).

https://doi.org/10.1016/j.segan.2024.101561
Received 30 May 2024; Received in revised form 15 October 2024; Accepted 25 October 2024
Available online 7 November 2024

Nomenclature

General

t, k	Time, discrete time-step
s	Laplace variable
T_s	Sampling period
$\mathbf{I}$	Identity matrix
S	Apparent power
ω, f, f_{LSO}, f_0	Angular frequency, frequency, optimisation frequency, nominal frequency
p^*, p_e, p_{PFC}	Power setpoint, electrical power, power due to primary frequency control action
J, H, H_n, H_{dP}	Moment of inertia, inertia constant, nominal inertia, RoCoP-based inertia

LSO-DREM procedure

H_c, H_{LSO}	Control inertia, optimisation inertia
$G(s)$	Transfer function of the primary frequency control
R	Droop constant
τ, τ_z, τ_p	Time constants of G(s)
J	Objective function
t_w	Time window for the optimisation
N	Number of samples within t_w
H	Lag operator
t_d	Time delay for H
$\mathbf{x}$, x_1, x_2	Vector and variables of the regressor
$\xi_{1,2,3}$	Coefficients of the regressor
λ	Learning rate
α	Filter parameter
ε_H	Threshold for ΔH
t_H	Time duration of ε_H
ε_P	Threshold for disturbance detection
e	Parametric error

Auxiliary symbols

$\gamma(t)$, $\Gamma(s)$	Relationship between frequency and electrical power
$a_{1,2}$, $b_{1,2,3}$, $h_{1,2,3}$, $k_{1,2,3}$, $r_{1,2,3}$	Auxiliary variables to define $\gamma(t)$ and $\Gamma(s)$
$\mathbf{A}$, $\mathbf{B}$, $\mathbf{Z}$, ∂	Vectors, matrices and variables of known quantities for the regression construction

1.2. Literature review

There are several ways to classify inertia estimation methods according to their characteristics [6–10]: state (static or dynamic); time horizon of interest (online, offline, forecast); type of data (large disturbance data, ambient data, micro disturbance data); method employed (model based, measurement based).

Static methods [11,12] rely on operating schedules or full system monitoring, often dependent on the availability of synchronous generator data. However, they may not be suitable for power systems with limited observability and a high penetration of distributed resources providing inertial response. Dynamic methods, on the other hand, overcome the disadvantages of static methods by directly analysing the dynamic behaviour of the system. This allows for a more accurate and up-to-date characterization of the inertia. For this reason, most of the methods proposed in recent literature are dynamic.

Offline methods [13,14], also known as post-mortem, typically analyse large disturbance events and are based on historical data, whereas online methods monitor inertia in real time using readily available measurements. A key advantage of offline methods is the ability to perform data processing and inertia estimation without concern for computational time. Online methods [15–27] offer the advantage of real-time (or close to real-time) awareness of the system state, allowing system operators to make adaptive adjustments based on current conditions. Another useful resource comes from predictive methods [12,28–30]. By using such methods, operators can take preventive actions to maintain system stability margins based on expected future conditions.

In terms of data type, large disturbance-based methods [13–18] rely on events that produce large frequency variations, such as faults, connection/disconnection of large generators or loads, etc. The accuracy of these methods typically depends on precise knowledge of the disturbance characteristics (size, timing). Moreover, the inertia information cannot be updated in real time. In contrast, ambient data-based estimation methods [19–25] use measurements obtained under normal operating conditions, taking advantage of the normal fluctuations of load and generation in the system. This feature makes them more flexible to adapt to changes in the network topology. Typically, methods based on ambient measurements also work with large perturbations, but not vice versa. Microperturbation-based methods [26,27] use a probe signal with known characteristics. This approach requires additional equipment, which increases the complexity of the implementation.

Considering the above characteristics, continuous awareness of the system inertia level is provided by dynamic online methods based on field data. This paper focuses on an inertia estimation method with these characteristics. In terms of the method employed, model-based methods [15,16,19,20,26] use dynamic models of varying complexity and adopt optimization algorithms, Kalman filters, state-space models, and transfer functions to estimate inertia and other parameters. These methods suffer from parameter uncertainties and the accuracy of the estimation depends on the models used. In contrast, measurement-based methods [17,21–24,27] do not require complex model representations and often use only the swing equation. However, they are susceptible to measurement noise.

The methods proposed in [18,25] are difficult to categorize as purely measurement based. Both methods are based on the swing equation but do not require the definition of model parameters. The method proposed in [18] is capable of tracking inertia with high accuracy. However, it depends on the accurate estimation of the rate of change of power (RoCoP) and frequency. In particular, the frequency is estimated using the frequency divider formula, which is based on the augmented matrix of the network and the knowledge of the generator impedances. In [25], a regression model is constructed from the swing equation, based on the dynamic regression extension and mixing (DREM). The model is based on a steam turbine unit and includes a single-pole transfer function to represent the dynamics of the primary frequency control (PFC). The method is tested during small disturbances associated with rescheduling events and shows good performance. The main limitation for the application of this approach lies in the assumption that the parameters of the PFC dynamics characterisation are known. To overcome this limitation, an extension of the method has been preliminarily proposed in [31]. The extension consists in estimating the unknown PFC parameters by means of a least-squares optimisation (LSO). In addition, a one-zero two-pole transfer function provides a more generalised model of PFC dynamics, enabling the representation of various types of power plants. In [31], the optimisation is based on an iterative procedure using a dynamic Simulink model, which makes the process slow.

1.3. Contributions of the paper and organization

In this paper, the inertia estimation technique proposed in [31] is improved with the following features:

– The PFC dynamics are represented using an analytical formulation. This allows the optimisation phase of the algorithm to be significantly accelerated, increasing computational efficiency.
– A sensitivity analysis is performed to evaluate the influence of the DREM parameters on the estimator's performance. This analysis made it possible to establish a criterion indicating the need to update the PFC parameters. This improvement allows the automation of the entire estimation process, making it suitable for the practical use. It also provides useful insights into the DREM characteristics for this application.

The proposed LSO-DREM procedure is tested on the IEEE 39-bus system. The tests consider load variations under normal operating conditions, load and generation steps in different inertia conditions, and the impact of CISs controlled in both grid-following and grid-forming modes. The performance of the LSO-DREM procedure is compared with the results obtained using the algorithm proposed in [18]. Real-time simulations are performed to validate the implementation.

The paper is organised as follows. Section 2 describes the application. Section 3 presents the methodology of the inertia estimation algorithm, including the optimisation and the regression procedures. In Section 4 the sensitivity analysis is performed and the criterion for updating the PFC parameters is defined. The results of the scenarios simulated on the IEEE 39-bus system are presented in Section 5. The real-time implementation of the algorithm is included here. Finally, Section 6 concludes the paper.

2. Application description

Fig. 1 shows the inertia estimation process. The inputs to the algorithm are measurements of system frequency $\widetilde{f}$ and total electric power injected by generators $\widetilde{p}_e$, and the output is the estimated inertia of the power system, denoted as $\widehat{H}$. Throughout the paper, the tilde ($\widetilde{u}$) refers to measured quantities, while the hat ($\widehat{u}$) refers to estimated quantities.

The optimisation stage identifies the parameters of the PFC dynamics (developed in Section 3.2) and the regression stage tracks the inertia value in real time (developed in Section 3.3). A control block checks the PFC parameters are up-to-date. Whenever it detects a change in the dynamics, a request to update the parameters is sent to the optimiser. The main contributions of this paper are those marked in the orange blocks, and the details of the algorithm are shown in Fig. 2.

The DREM method uses a regression and gradient algorithm to estimate inertia. However, as mentioned above, the parameters of the primary frequency control are needed to construct the regression model. To solve this problem, the optimisation stage estimates these parameters ($\widehat{\tau}$, $\widehat{\tau}_z$, $\widehat{\tau}_p$). The dynamic behaviour of the primary frequency control is represented by an analytical form, in which the frequency variation is expressed as a function of the electrical power variation and the PFC parameters. Optimisation-based PFC identification follows the following steps:

(a) frequency variation $\Delta\widetilde{f}$ and electrical power variation $\Delta\widetilde{p}_e$ are measured over time window t_w when a disturbance occurs;
(b) frequency variation Δf is evaluated by using the analytical expression;
(c) the difference between $\Delta\widetilde{f}$ and Δf is minimised and the PFC parameters are obtained.

The DREM stage constantly tracks the inertia, while the optimisation stage is started only when it is necessary to update the PFC parameters, which are determined by the following conditions:

– ΔH condition: A control value ($\widehat{H}_c$) is estimated by a parallel gradient algorithm with different regression parameters. Estimated inertia $\widehat{H}$ and control value $\widehat{H}_c$ diverge only if the PFC parameters do not correspond to the real dynamics of the system (details are given in Section 4.2). If the difference between these two values exceeds a threshold (ε_H), the optimisation stage must be performed to estimate new PFC parameters. To avoid activating this condition during the transient state of the estimator, it is required that the threshold be exceeded for a certain time interval (t_H).

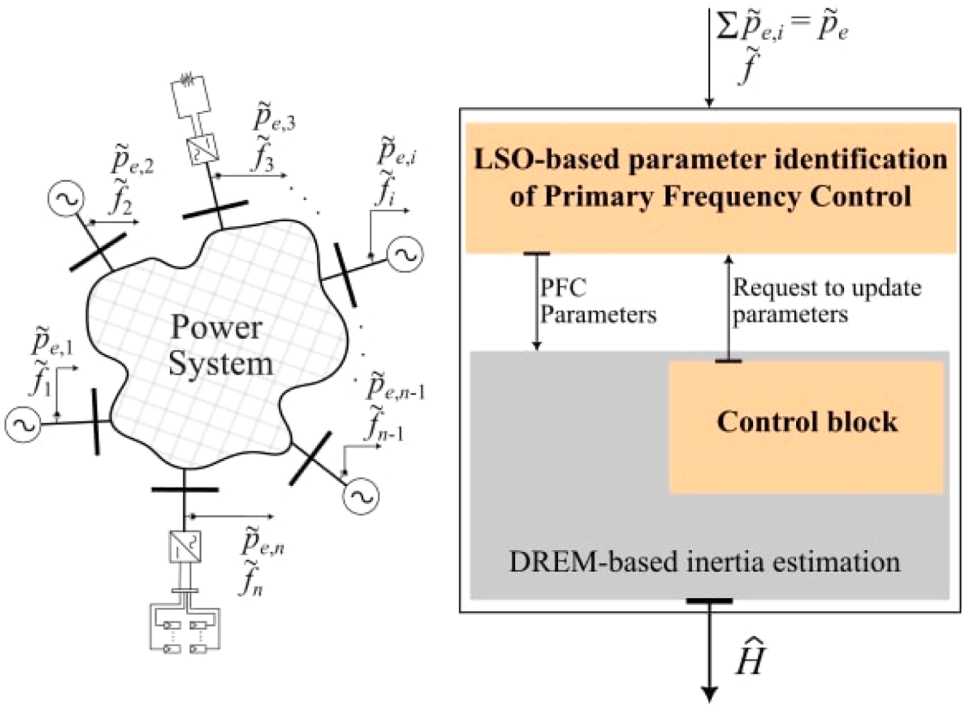

Fig. 1. Scheme of the inertia estimation for a generic power system.

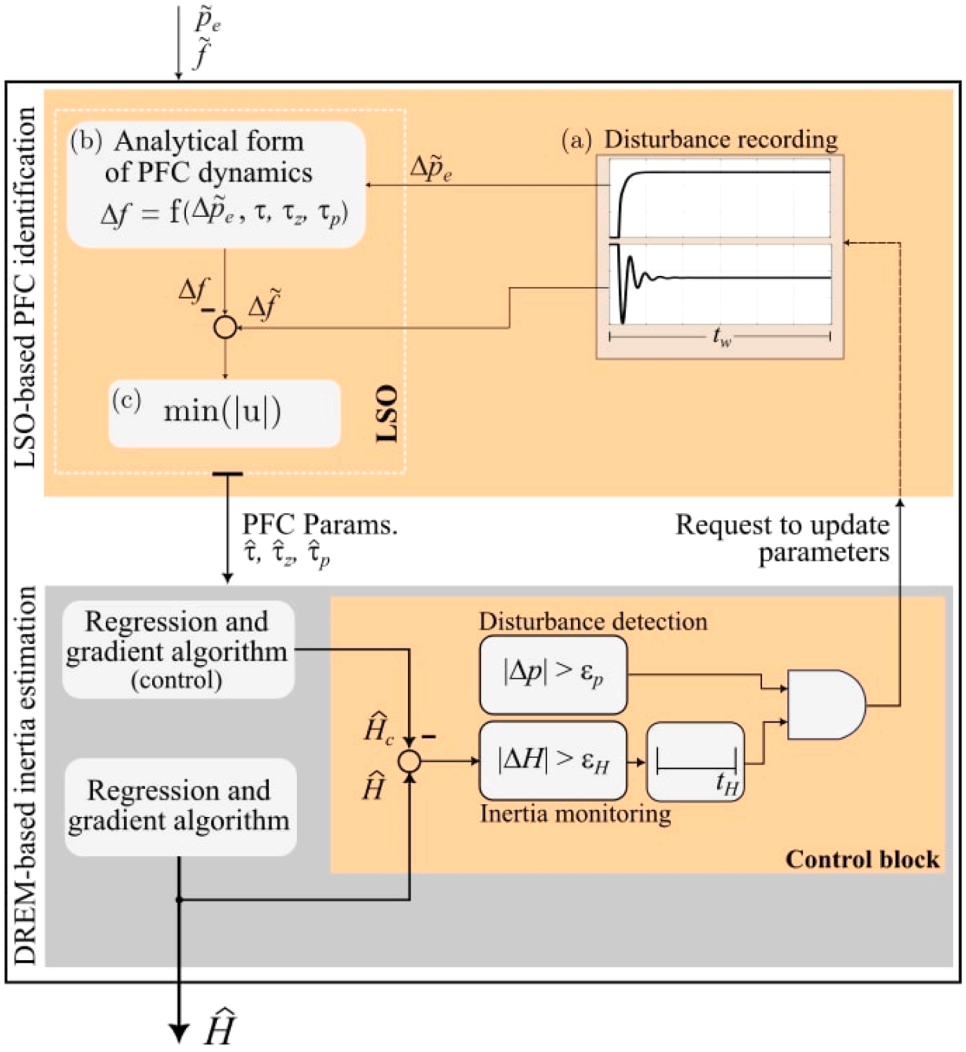

Fig. 2. Block diagram of the proposed LSO-DREM inertia estimation algorithm.

– Δp condition: To ensure the accuracy of the PFC parameters, the optimisation is performed when a significant disturbance occurs. The LSO is therefore executed when Δp is greater than a tolerance (ε_P).

3. Mathematical formulation

Section 3.1 briefly recalls the swing equation and introduces the general representation of the primary frequency control. Section 3.2 derives the analytical expression of the PFC dynamics and illustrates the optimisation procedure. Section 3.3 constructs the regression model from the swing equation based on the DREM procedure.

3.1. Swing equation

The swing equation of a generator expressed in per unit (pu) is given by [32]:

$$2H\dot{\omega} = \frac{\Delta p}{\omega}, \tag{1}$$

where the damping has been neglected [6,9]; ω is the angular frequency and $\dot{\omega}$ its time derivative; and Δp is the power unbalance.

The power unbalance can be expressed as

$$\Delta p = p^* + p_{PFC} - p_e, \tag{2}$$

where p^* is the power setpoint; p_{PFC} is the primary frequency control action; and p_e is the electrical power. Eq. (2) represents the actual unbalance between the load and the mechanical power, which accounts for the deviation from the set point due to the action of the governor. The whole power system behaviour can be represented by the aggregated swing equation (ω=f in pu):

$$\dot{f} = \frac{1}{2H}\frac{p^* + p_{PFC} - p_e}{f}. \tag{3}$$

While p_e and f can be measured, direct measurement of p^* and p_{PFC} is not possible. If the aggregated droop constant is known, the steady-state value of p_{PFC} can be derived. However, in the case of synchronous generators, the dynamic behaviour of p_{PFC} depends on that of the turbine-governor system, which is often unknown to the system operator. Similarly, for CISs, the dynamics of p_{PFC} depend on the characteristics of the source and the control system, which are also unknown.

3.2. Identification of PFC dynamic parameters

This section outlines the process implemented to determine the dynamics of the primary frequency control. This is one of the two main contributions of the paper.

In general, p_{PFC} can be represented in the Laplace domain as

$$p_{PFC}(s) = -\frac{1}{R}G(s)(f - f_0), \tag{4}$$

where R is the droop constant and f_0 is the nominal frequency. The transfer function $G(s)$ represents the dynamics of the PFC. $G(s)$ tends to 1 when s goes to zero, therefore the steady-state contribution of the PFC is equal to $-\Delta f/R$.

For small disturbances the frequency is close enough to its nominal value. Hence, (3) can be expressed as

$$s\Delta f(s) = \frac{1}{2H}(\Delta p_{PFC} - \Delta p_e). \tag{5}$$

The dynamic model used for the PFC dynamic identification can be derived from (4) and (5) as

$$\Delta f(s) = \Delta p_e(s)\cdot\frac{-1}{2Hs + \frac{1}{R}G(s)}. \tag{6}$$

The dynamic model with one pole and one zero proposed in [33] is suitable for application in analyses that focus on the frequency dynamics of the system [34]. However, this low-order model assumes the shape of the frequency response, as a result of a load disturbance, is mostly affected by the action of reheat steam turbine generators. The second-order function obtained by adding a second pole offers a more general representation of the system dynamics, allowing different types of generators to be assessed, such as those driven by hydraulic turbines [32]. Therefore, in this paper the aggregated PFC dynamics are represented with one zero and two pole transfer function $G(s)$:

$$G(s) = \frac{1}{1+\tau s}\cdot\frac{1+\tau_z s}{1+\tau_p s}, \tag{7}$$

where τ, τ_z and τ_p are the corresponding time constants and represent the PFC parameters to be estimated. $G(s)$ represents both governor and turbine dynamics. Then (6) can be rewritten as

$$\Delta f(s) = \Gamma(s)\cdot\Delta p_e(s), \tag{8}$$

where the transfer function $\Gamma(s)$ is defined as:

$$\Gamma(s) = -\frac{1}{2Hs + \frac{1}{R}\cdot\frac{1}{1+\tau s}\cdot\frac{1+\tau_z s}{1+\tau_p s}}. \tag{9}$$

This transfer function represents the dynamic relationship between frequency and electrical power. However, in order to use the frequency and power measurements, it is necessary to express the relationship in the time domain. This is achieved by applying the convolution theorem to (8):

$$\Delta f(t) = \gamma(t) \otimes \Delta p_e(t), \tag{10}$$

where $\otimes$ is the convolution operator and $\gamma(t)$ is the inverse Laplace transform of $\Gamma(s)$. It characterises the time domain representation of the PFC dynamics. The derivation of $\gamma(t)$ is detailed in Appendix A, and its final form is

$$\gamma(t) = -R\cdot(k_1 e^{-r_1 t} + k_2 e^{-r_2 t} + k_3 e^{-r_3 t}), \tag{11}$$

where $k_{1,2,3}$ and $r_{1,2,3}$ are functions of H, R, τ, τ_z and τ_p.

To estimate τ, τ_z and τ_p, a parameter identification process is performed based on a least-squares optimisation technique. The objective function to be minimised is the difference between the measured frequency variation and the analytical formulation resulting from (10)–(11):

$$J = \min \|\widetilde{\Delta f} - \Delta f\|_2. \tag{12}$$

The optimisation is performed over a time window t_w that is appropriately sized to include the entire PFC action. For the implementation, the equations must be discretised. If T_s is the sampling period of the measurements, then (10)–(12) are expressed as

$$\Delta f(k) = \Delta\tilde{p}_e(k) \otimes \gamma(k), \tag{13}$$

$$\gamma(k) = -R\cdot\left(k_1 e^{-r_1 kT_s} + k_2 e^{-r_2 kT_s} + k_3 e^{-r_3 kT_s}\right), \tag{14}$$

$$J = \min \sum_{k=1}^{N} (\Delta\widetilde{f}(k) - \Delta f(k))^2, \tag{15}$$

where k is the discrete time step and N is the number of samples within the time window t_w. An estimated frequency deviation, denoted in the following as $\Delta\widehat{f}_{LSO}$, is obtained from the solution of the optimisation problem.

The LSO procedure is illustrated in Fig. 3. In addition to estimating $\widehat{\tau}$, $\widehat{\tau}_z$ and $\widehat{\tau}_p$, the optimisation also estimates the inertia ($\widehat{H}_{LSO}$). Since (11) is a linear combination of exponential functions, (12) is evaluated using a recursive convolution scheme, which drastically reduces the computation time. However, real-time tracking of inertia is not efficient using this method alone, as the optimisation requires a significant disturbance to obtain accurate results.

3.3. Dynamic regression extension and mixing

To achieve real-time inertia tracking, the method used in this paper is based on the DREM procedure. To keep the paper self-contained, the mathematical formulation of the DREM is given in Appendix B. In this section, only those aspects relevant to the LSO-DREM algorithm are presented.

The DREM constructs a linear regression based on (3), which can be rewritten as

$$\dot{f} = \frac{1}{H}\left(\frac{1}{2}\frac{p_{PFC} - p_e}{f}\right) + \frac{p^*}{H}\left(\frac{1}{2f}\right). \tag{16}$$

Once p_{PFC} is known, the unknown parameters are H and p^*. To match the number of equations to the number of unknown parameters, the regression is extended by applying a dynamic operator to the original regressor. The extension is obtained by applying the lag operator $\mathscr{H}$:

$$[\mathscr{H}(\cdot)](t) = (\cdot)(t - t_d), \tag{17}$$

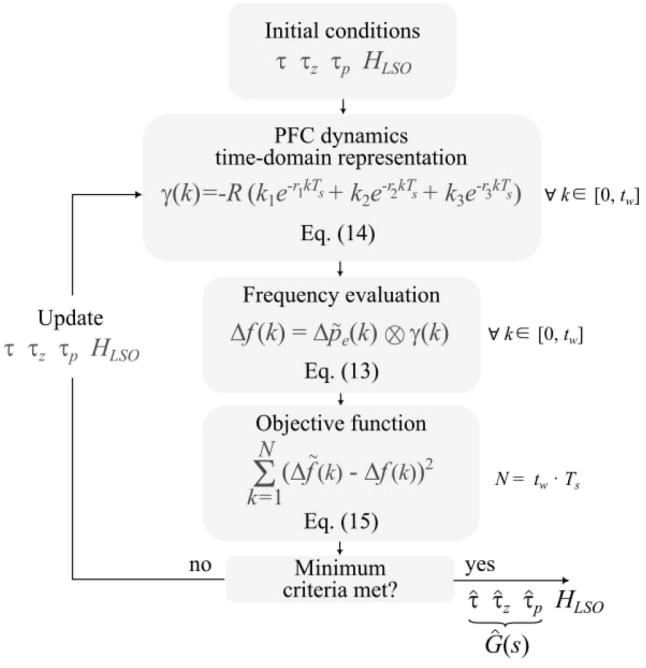

Fig. 3. Flowchart of the least-squares optimisation.

where t_d is the time delay. This operation gives a second regression equation:

$$\mathscr{H}\left(\dot{f}\right) = \frac{1}{H}\cdot\mathscr{H}\left(\frac{1}{2}\frac{p_{PFC}-p_e}{f}\right) + \frac{p*}{H}\cdot\mathscr{H}\left(\frac{1}{2f}\right). \tag{18}$$

For the practical implementation of the regression expressed in Eqs. (16) and (18), a filter is used to avoid the derivative operator applied to the frequency. Further details are given in Appendix B. Combining the two regression Eqs. (16) and (18) gives a regression of general form:

$$\mathbf{A} = \mathbf{B}\,\mathbf{x}, \tag{19}$$

where $\mathbf{A}$ is a 2×1 vector and $\mathbf{B}$ is a 2×2 matrix, both composed of known quantities; $\mathbf{x}=[x_1,x_2]$ is the vector of variables to be estimated, i.e. $x_1 = 1/H$ and $x_2 = p^*/H$ in (18).

The mixing procedure then decouples the regressions, allowing the two unknown parameters to be estimated independently. The final form of the regression is:

$$\mathbf{Z} = \partial\cdot\mathbf{x}, \tag{20}$$

where $\mathbf{Z}$ is a 2×1 vector and ∂ is a scalar, both of which are known quantities.

Parameters $\hat{x}_1$ and $\hat{x}_2$ can be estimated from (20) using the gradient algorithm [35]. The discretised law describing the update of $\hat{x}_1$ and $\hat{x}_2$ is

$$\Delta\hat{x}_i(k+1) = \lambda_i\partial[Z_i - \partial\hat{x}_i(k)]T_s \quad i=1,2, \tag{21}$$

where λ_i is the learning rate of the gradient algorithm for each process. For simplicity, the same value of λ is used for all processes in this paper.

The variables of interest are derived from the estimated parameters as

$$\begin{aligned}\hat{H} &= (\hat{x}_1)^{-1}\\ \hat{p}^* &= \hat{H}\cdot\hat{x}_2.\end{aligned} \tag{22}$$

The DREM procedure is shown in Fig. 4. The focus is on the inertia, so the estimation of $p*$ is not considered. To reduce the effects of transients during the estimation, the DREM output is saturated ($H_{\max}$ and $H_{\min}$) and filtered. The purpose of the saturation is only to avoid unrealistic values and it has no effect on the performance of the algorithm.

The two parameters that determine the behaviour of the DREM are time delay t_d, and learning rate λ. In Section 4.2 a sensitivity analysis is performed to assess their impact.

4. Sensitivity analysis

4.1. Preliminary results

The performance of the LSO and the DREM procedures is first tested separately on the simplified system of Fig. 5. The equivalent system is simulated using a 10 GW synchronous generator driven by a steam turbine (as in [36]). The nameplate inertia constant (H_n) is 6 s and the droop is 5 %.

To test the optimisation performance, a 200 MW (0.02 pu) load step

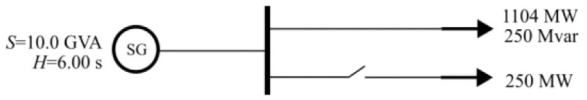

Fig. 5. Simplified test system for the sensitivity analysis of regression-based estimation.

is simulated. Typically, the dynamics of the primary frequency response are on the sub-minute timescale. Therefore, the LSO is performed over a 60 s time window. The estimated parameters of $\widehat{G}(s)$ are given in Table 1 and the correspondence between $\Delta\widetilde{f}$ and $\Delta\widehat{f}_{LSO}$ is shown in Fig. 6. The real-time tracking of the inertia performed by the DREM is shown in Fig. 7, and the results are given in Table 2 along with the LSO estimated inertia. After the initial transient following the disturbance, the estimation algorithm stabilises at a constant value.

4.2. Sensitivity analysis

A sensitivity analysis of the DREM procedure is carried out to propose a criterion to determine when the PFC parameters must be updated (e.g., due to the connection of other sources that modify the PFC dynamic characteristics of the system). This allows the integration between the two algorithms, which is the second main contribution of the paper.

Firstly, it is of interest to evaluate the performance of the DREM when either the inertia or the PFC dynamics change. Two scenarios are defined.

- Scenario A – Variation of the inertia constant: the inertia of the equivalent system is changed to 5 s. The PFC dynamics are the same as in the base case.
- Scenario B – Variation of the PFC dynamics: the PFC dynamics are changed by varying the time constants of the governor. The inertia is the same as in the base case (i.e., 6 s).

The performance of the DREM is assessed for both cases using the parameters from Table 1. A 200 MW load step at t=0 s is introduced and the estimated inertia for both scenarios is shown in Fig. 8. For scenario A, the estimated inertia is 4.928 s (1.44 % error), and for scenario B it is 6.537 s (7.72 % error). These results show that the DREM is accurate when the PFC dynamic parameters are up-to-date. However, its accuracy decreases when these dynamics change without the parameters

Table 1
LSO and DREM Parameters.

LSO	τ	τ_z	τ_p
Value	0.288	1.650	10.149
DREM	λ	t_d	
Value	10^9	2 s	

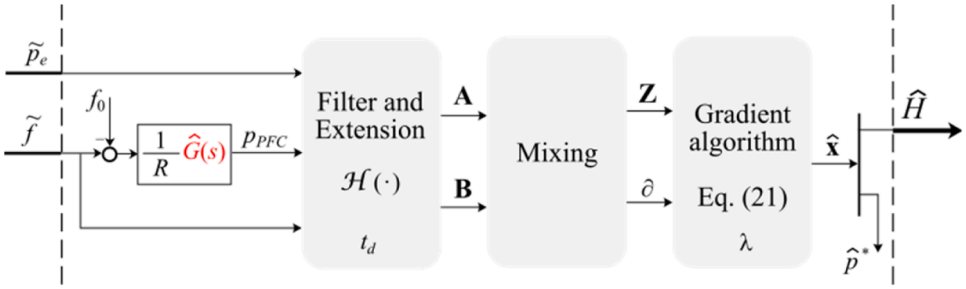

Fig. 4. Scheme of the dynamic regression extension and mixing procedure.

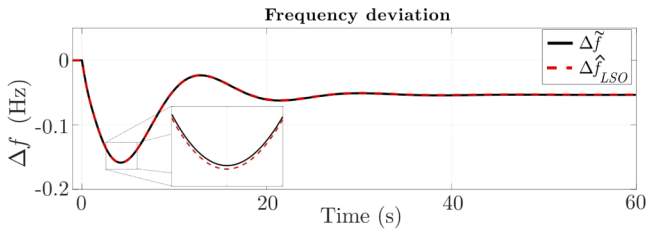

Fig. 6. Comparison between frequency measured ($\Delta\tilde{f}$) and estimated by the LSO ($\Delta\hat{f}_{LSO}$).

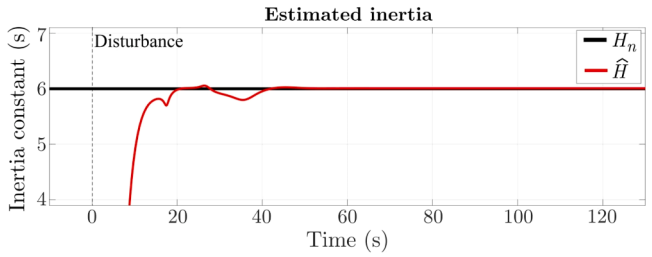

Fig. 7. Real-time inertia tracking with the DREM procedure.

Table 2
Estimated Inertia by LSO and DREM.

	$\hat{H}$	error
LSO	5.940	1.00 %
DREM	6.008	0.13 %

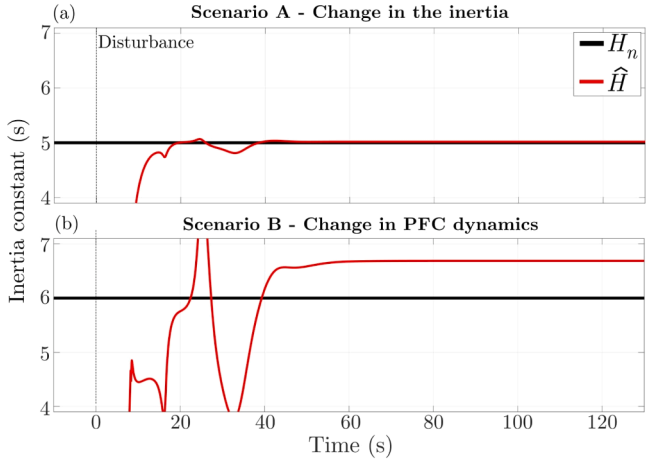

Fig. 8. Estimated inertia for Scenarios (a) A and (b) B.

being updated.

To further explore the characteristics of DREM, the influence of time delay t_d and learning rate λ are examined, considering the base case and the two scenarios previously described. To avoid the numerical divergence of $\hat{H}$,$H_{\min}$ and $H_{\max}$ are set to 0 and 10 s, respectively. These limits do not affect the performance of the algorithm.

4.2.1. *Influence of the time delay*

The time delay should be within the inertial response window of the system. Fig. 9 illustrates the effect of t_d on the estimated inertia. The shaded area indicates a ±5 % error margin. The blue dots indicate those estimates where parametric error $\hat{e}$ is large, making the estimate unreliable.

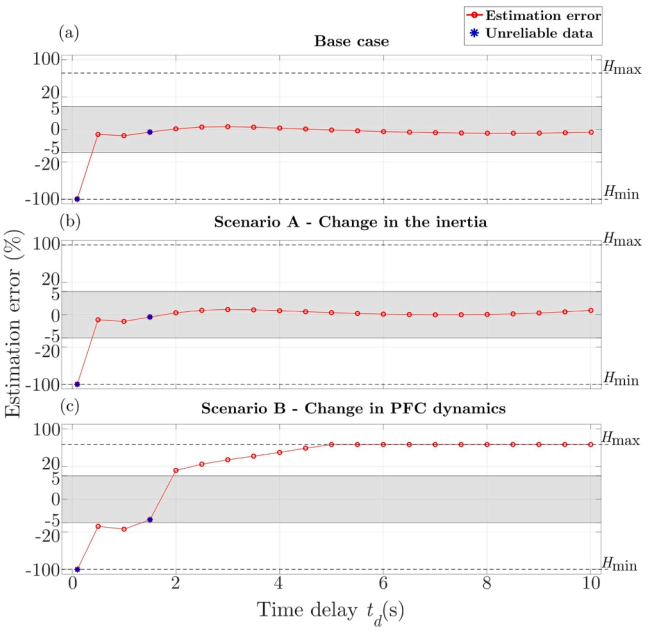

Fig. 9. Effect of time delay on estimated inertia. Estimation errors for different values of t_d for (a) the base case; (b) Scenario A; (c) Scenario B.

In both the base case and Scenario A (PFC dynamics have not changed since the optimisation), the estimated inertia is not significantly affected by the choice of t_d. However, in Scenario B the effect is significant. For values of t_d greater than 2 s, the error is large. This dependence of the estimated inertia for different t_d values when the PFC dynamics change is used as a criterion to determine the need to update the PFC parameters. For this purpose, a parallel gradient algorithm with different t_d is used to estimate the control inertia $\hat{H}_c$ (see Fig. 2).

4.2.2. *Influence of the learning rate*

The learning rate determines the convergence speed of the gradient algorithm. Large values make the estimation procedure faster, but too large values can cause overshooting and increase the sensitivity to noise.

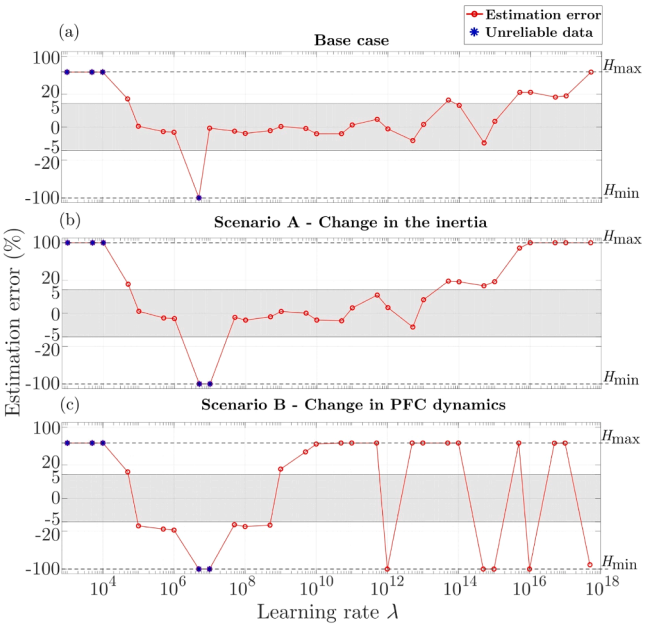

Fig. 10. Effect of the learning rate on the estimated inertia. Estimation errors for different values of λ for (a) the base case; (b) Scenario A; (c) Scenario B.

Fig. 10 illustrates the effect of λ on the estimated inertia.

For the base case and Scenario A the estimation error is minimal for a wide range of λ values ($5{\cdot}10^4$–10^{15}). However, for scenario B, the influence of λ becomes significant. The errors are large for several values of λ, making the estimation unreliable in these conditions.

The algorithm is stable for a wide range of λ values as long as the PFC parameters are updated. This dependence could also be used as a criterion for updating the PFC parameters.

5. Test cases

To evaluate the algorithm performance, the 10-generator 39-bus IEEE system shown in Fig. 11 is implemented in Matlab/Simulink [36]. The injected active power is measured for each generator and the frequency is obtained from a phase-locked loop (PLL) module connected to the bus of generator 1.

The system inertia constant H_n is calculated using:

$$H_n = \sum_i H_i{\cdot}S_i \Big/ \sum_i S_i, \tag{23}$$

for all i-th generators effectively connected to the grid. When all synchronous generators are connected to the system, this value is 4.208 s. The PFC and LSO-DREM parameters are given in Table 3.

For the performance tests, generators no. 4, 7, and 8 of Fig. 11 (marked in red) are operated to vary the dynamics of the system. In the first case, these generators are disconnected. In the second case, they are replaced by CISs with the power converters controlled in either grid-following or grid-forming mode. In the grid-following mode, the inverter controls the active and reactive power to follow a reference. In the grid-forming mode, the frequency is controlled by implementing a virtual synchronous machine (VSM) technique with damping [37], and the voltage is controlled with a droop control strategy. The LSO-DREM algorithm is also tested under normal operating conditions, considering load and frequency variations.

5.1. Disconnection of synchronous generators

This scenario simulates a sequence of disturbances and the disconnection of the three generators 4, 7, and 8. This test illustrates the algorithm operation. The result provided by the algorithm is compared to the estimated inertia based on the method proposed in [18] (designed as $\widehat{H}_{dP}$ as it is a by-product of the RoCoP estimation).

The estimated values of the inertia constant and the control variables of interest are shown in Fig. 12 including the control value $\widehat{H}_c$. The inertia is first estimated after a disturbance at t=5 s. At t=100 s, the three generators are disconnected, causing the change in the PFC dynamics. The algorithm detects the change in inertia and the ΔH condition is activated due to the change in the PFC dynamics. At t=300 s, a disturbance is detected and recorded for the time window t_w. Optimisation is then triggered, and the PFC parameters are updated. Finally,

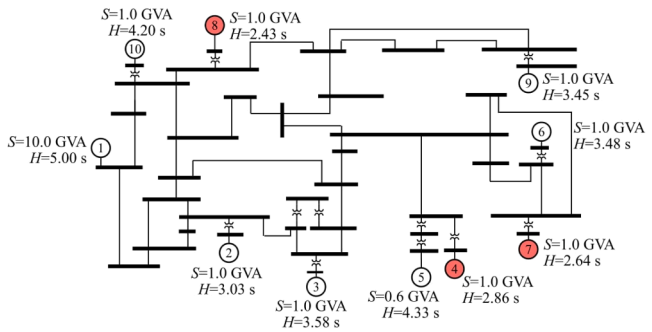

Fig. 11. IEEE 39-bus test system.

Table 3
LSO-DREM parameters.

LSO					
Parameter		τ	τ_z	τ_p	t_w
Value	①	0.356	1.564	9.738	60 s
	②	0.363	1.590	9.842	
DREM					
Parameter		λ		t_d	
Value		10^9		1 s	
Control					
Parameter		t_d	ε_H	t_H	ε_P
Value		3 s	0.25 s	60 s	15 MW

①: Base case; ②: After the generation disconnection.

after a disturbance at t=550 s, the inertia is estimated with the new PFC parameters. The accuracy of the algorithm is tested at three times, as shown in Fig. 12:

A: before the generators are disconnected;

B: after the disconnection but before updating the PFC parameters;

C: after updating the PFC parameters.

When the generators are disconnected the system inertia constant H_n increases to 4.509 s, even though the total moment of inertia decreases, as shown in Table 4. This increase occurs because the base power, which acts as the denominator in (23), decreases.

Table 4 compares the inertia constants estimated by using the different methods and their corresponding relative errors. It shows that the considered methods are sufficiently accurate in estimating the inertia. The RoCoP-based method has the important advantage of working without the need for parameter updates. However, this method relies on the accurate estimation of the rotor frequency of each generator due to its dependence on the second derivative of the frequency. For the calculation of the inertia constants given in Table 4 the rotor frequency values were assumed to be known. However, the RoCoP-based method did not work correctly using the PLL measurement; instead, the LSO-DREM works well with the frequency measured at a single point in the system, which is a major advantage.

5.2. Normal operating conditions

The algorithm is tested under normal operating conditions. Fig. 13(a) shows the system frequency caused by the load variation. Fig. 13(b) shows the comparison between the estimated inertia and H_n. The mean value of the estimated inertia in the last 200 s (to neglect the initial transient) is 4.267 s, giving an error of 1.41 %.

5.3. Algorithm performance with unchanged PFC dynamics

Although the DREM does not use the value of $\widehat{H}_{LSO}$ directly in the estimation process, it is correlated with the values of $\widehat{\tau}$, $\widehat{\tau}_z$ and $\widehat{\tau}_p$. To evaluate such dependency, the algorithm is tested in the presence of a highly variable load. The three generators are disconnected at t=160 s changing the PFC dynamics. The results are shown in Fig. 14. In this scenario, the difference between $\widehat{H}$ and $\widehat{H}_c$ is small and not persistent. Therefore, the condition ΔH is not satisfied and the optimiser is not triggered. Nevertheless, the DREM is able to track the change in system inertia.

As long as $\widehat{H}$ and $\widehat{H}_c$do not diverge, the accuracy of the inertia estimated by the proposed algorithm is adequate. However, a periodic estimation of the PFC parameters could be performed independently of the activation of the ΔH condition.

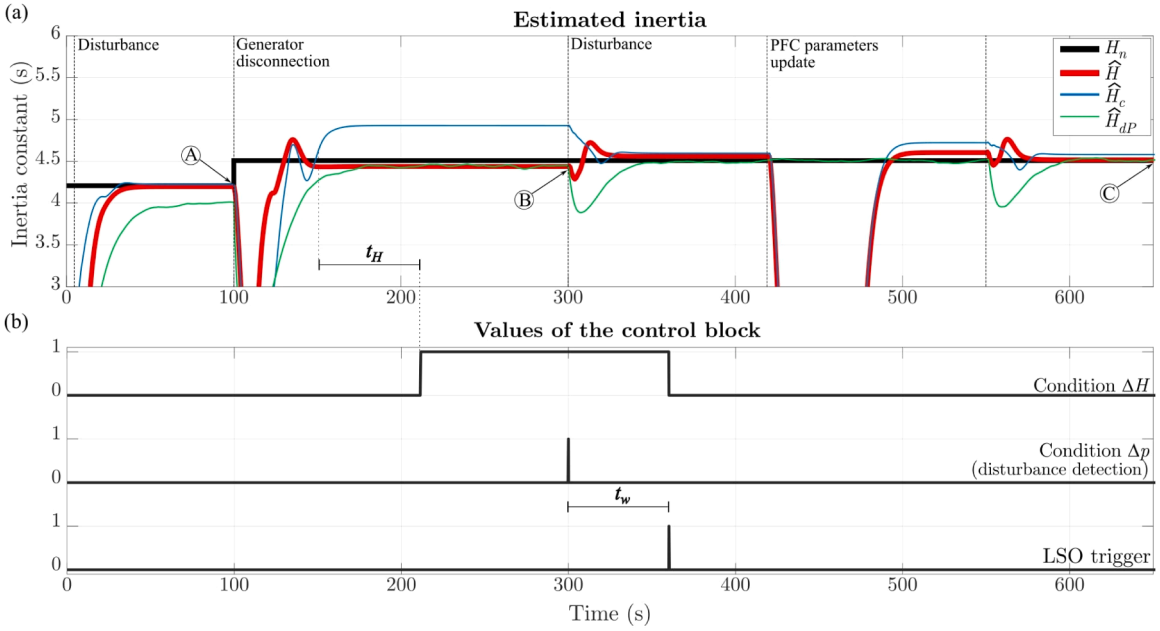

Fig. 12. Performance of the LSO-DREM algorithm in the case of synchronous generator disconnection: (a) estimated inertia and (b) control block values.

Table 4
Estimated inertia constant.

	H_n	LSO		LSO-DREM		RoCoP	
		$\widehat{H}_{LSO}$	error	$\widehat{H}$	error	$\widehat{H}_{dP}$	error
A	4.208 (S_b=18.6 GVA) $J = 1.586$ MJ s^2	4.231	0.55 %	4.197	0.26 %	4.011	4.68 %
B	4.509 (S_b=15.6 GVA)		6.17 %	4.438	1.58 %	4.449	1.32 %
C	$J = 1.425$ MJ s^2	4.491	0.40 %	4.517	0.18 %	4.516	0.16 %

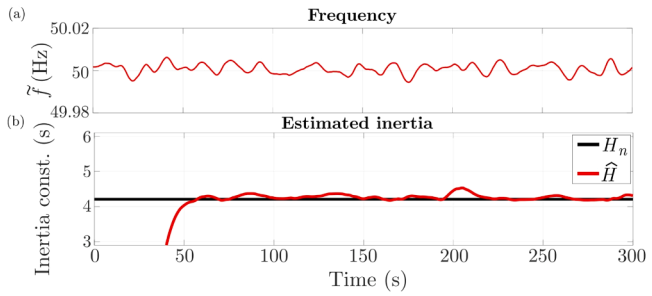

Fig. 13. (a) Frequency variation and (b) estimated inertia under normal operating conditions.

5.4. Converter interfaced sources

To evaluate the impact of converters, the three generators no. 4, 7, and 8 of Fig. 11 are replaced by CISs controlled in either grid-following or grid-forming mode. A 250 MW load step is introduced at t=0 s. The frequency of the system and the estimated inertias are shown in Fig. 15 and in Table 5.

For the grid-following case the inertia is $H_{n,GFL}$=3.782 s, considering the contribution of the CIS zero in (23). The estimated value is 3.781 s, resulting in a negligible error.

The grid-forming inverters are designed with the same inertia constant as the synchronous generators they replace. However, the primary response of the grid-forming inverters is faster than that of the synchronous generators [18,38], resulting in a lower frequency deviation and a lower rate of frequency change compared to the case without CIS.

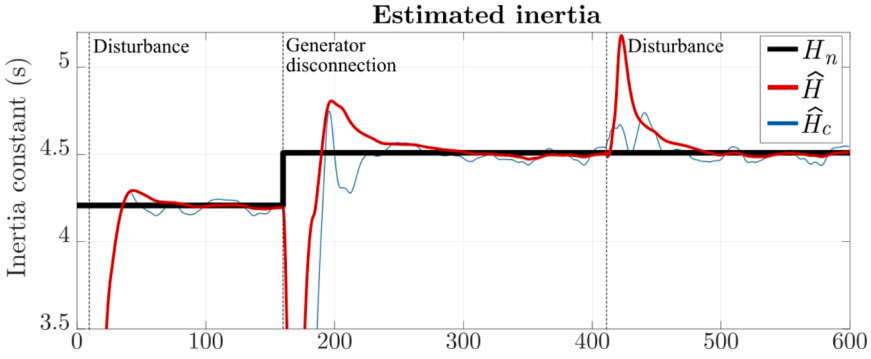

Fig. 14. Estimated inertia when the PFC dynamics are not updated after generator disconnection.

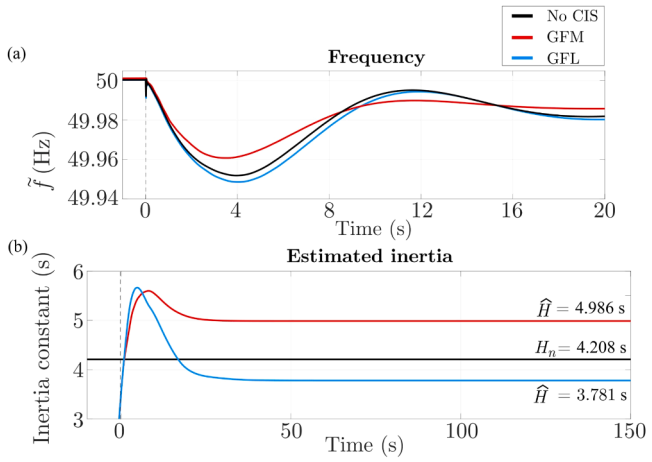

Fig. 15. Effect of CIS on (a) frequency and (b) system inertia. CIS are controlled in grid-following (GFL) or grid-forming (GFM) mode.

Table 5
Estimated inertia constant with converter-interfaced sources.

	H_n	LSO		LSO-DREM	
		$\widehat{H}_{LSO}$	error	$\widehat{H}$	error
GFL	3.782	3.765	0.45 %	3.781	0.00 %
GFM	4.209†	5.055	–	4.986	–

†This value does not consider the inertia effect provided by the droop action of GFM converters. Therefore, the error is not reported in this case.

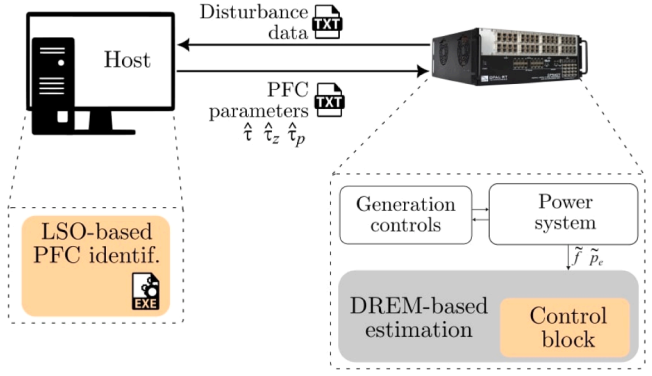

Fig. 16. Test of the LSO-DREM approach using a real-time simulator.

The droop effect of the GFM converters results in a higher effective inertia [39–41], as shown in Fig. 15. In this case, the nominal inertia is $H_{n,GFM}$=4.209 s as for the base case. However, this nominal value does not consider the inertia due to the above-mentioned droop action. An error for this would not be relevant for the present analysis and, therefore, it is not shown in Table 5. Future work should consider this aspect.

5.5. Real-time implementation

A real-time test was performed using an Opal-RT 4510 simulator.

The aim of this simulation is to validate the approach and confirm that the LSO-DREM algorithm can handle real-time computational tasks.

The implementation is shown in Fig. 16. In the proposed algorithm, the regression must run continuously while the optimisation is triggered only when required. For the real-time simulation, the optimisation is built into an executable file. The optimisation stage is executed asynchronously on the development computer (host). When executed, it writes the estimated PFC parameters into a text file. The regression algorithm then reads this file periodically (e.g., every 60 s). Similarly, the disturbance data required for the optimisation is written into a text file, which is read by the optimiser when it runs.

For the real-time simulation the system was divided into three subsystems: the power system (generators, transformers, lines, loads); the generator controls (governors and exciters); and the inertia estimation algorithm. A scenario similar to that described in Section 5.1 is simulated and the real-time results are shown in Fig. 17. The behaviour of the DREM without the output filter is also shown.

The estimated inertia values and the computation times required for a simulation of 800 s are given in Table 6. The time step is 2 ms. The main computation burden at each step of the simulation is the power system computation (an average time of 1.84 ms). The inertia estimation subsystem takes about 91.5 µs. This shows that the algorithm is well suited for a real-time implementation. Moreover, since the LSO-DREM algorithm relies solely on frequency and active power measurements, its resource consumption is not affected by the complexity or size of the system, making it scalable.

6. Conclusions

This paper presents a novel online inertia estimation algorithm consisting of two stages: an optimisation-based parameter identification and a regression-based inertia estimation. The optimisation stage estimates the parameters that characterise the dynamics of the primary frequency control (PFC). These parameters are then used by the regression stage to track the inertia constant of the system. A gradient algorithm is used to solve the regression.

The inertia estimation is based on the dynamic regression extension and mixing method already documented in the literature. However, such a method depends on the dynamic parameters of the primary frequency control, which are usually unknown. To overcome this problem, the integration of a parameter identification stage is here proposed. This allows the implementation of a fast optimisation stage where the differences between the measured frequency response during a disturbance and the frequency response derived from the analytical formulation are

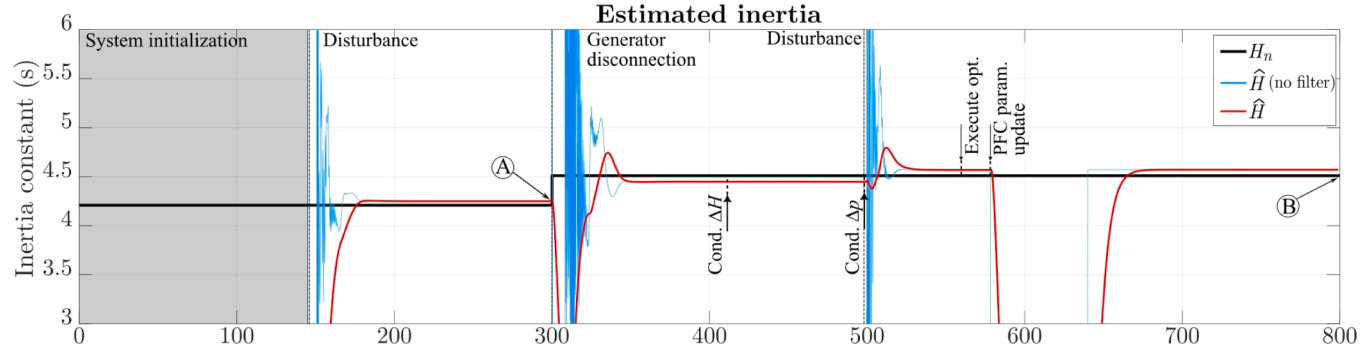

Fig. 17. Estimated inertia - Real-time results.

Table 6
Real-time results.

Computational times				
Subsystem	**Resource usage**	**Step-time**		
		Minimum	**Maximum**	**Average**
Power system	91.83 %	1831.55 µs	1846.49 µs	1836.63 µs
Generation controls	0.16 %	2.93 µs	3.68 µs	3.21 µs
DREM	4.57 %	91.23 µs	92.04 µs	91.50 µs
Inertia estimation				
	H_n	$\widehat{H}$	**Error**	
A	4.208 s	4.250 s	1.00 %	
B	4.509 s	4.570 s	1.35 %	

minimised. This analytical approach results in a highly efficient optimisation process that takes less than a second to determine the optimal set of parameters that accurately describe the PFC dynamics.

A sensitivity analysis was performed to evaluate the impact of two factors on the algorithm performance: the time delay of the operator (t_d) and the learning rate of the gradient algorithm (λ). When the PFC parameters are updated, the estimated inertia does not depend significantly on these two factors. However, when the PFC parameters are not updated, e.g., when a set of generators is disconnected, the estimated inertia is different for different values of t_d or λ. This property is used to decide when the PFC parameters need to be updated. In particular, a control gradient algorithm using a different t_d estimates the inertia in parallel with the main gradient algorithm. If the difference between the estimated values exceeds a threshold, the optimisation stage is triggered.

The performance of the proposed approach has been tested using the IEEE 39-bus benchmark network, under normal load variations, under large disturbances, and in the presence of converter-interfaced sources controlled in both grid-following and grid-forming modes. The change in the effective inertia when converter-interfaced sources are connected to the power system can be successfully identified. The results of the real-time simulations confirm the applicability of the algorithm, which is characterised by low computational times.

The influence of measurement noise, which is of particular interest for the estimation under normal load variations, is beyond the scope of this paper, but deserves specific investigation as well as the development of a method capable of identifying the individual contributions to the inertia from conventional generation, virtual inertia, and rotating loads.

CRediT authorship contribution statement

Fabio Tossani: Writing – review & editing, Software, Methodology, Formal analysis, Conceptualization. **Fabio Napolitano:** Writing – review & editing, Methodology, Conceptualization. **Andrea Prevedi:** Writing – review & editing, Software, Methodology, Conceptualization, Formal analysis. **Juan Diego Rios Peñaloza:** Writing – original draft, Software, Methodology, Formal analysis, Conceptualization. **Milan Prodanovic:** Writing – review & editing, Supervision, Methodology, Conceptualization. **Alberto Borghetti:** Writing – review & editing, Supervision, Methodology, Conceptualization.

Declaration of Competing Interest

The authors declare that they have no known competing financial interests or personal relationships that could have appeared to influence the work reported in this paper.

Acknowledgments

Comments by Prof. Carlo Alberto Nucci and Dr. Javier Roldán-Pérez gratefully acknowledged.

This work is developed in the framework of the REDESFUERTES project (PID2022–142416OB-I00), funded by MICIU/AEI/10.13039/501100011033. It is also supported in part by Italian Ministry of University and Research (MUR), Project code PE0000021, CUP "J33C22002890007". Project title “Network 4 Energy Sustainable Transition – NEST”.

Appendix

A. Inverse Laplace Transform of PFC Dynamics

A rearrangement of the expression for $\Gamma(s)$ in (9) yields:

$$\Gamma(s) = -R\cdot\frac{1+a_1 s+a_2 s^2}{1+b_1 s+b_2 s^2+b_3 s^3}, \tag{24}$$

where

$$\begin{aligned} &a_1=\tau+\tau_p;\ a_2=\tau\tau_z;\\ &b_1=2HR+\tau_z;\ b_2=2HRa_1;\ b_3=2HRa_2. \end{aligned} \tag{25}$$

The term (-R) is omitted for simplicity and will be reintroduced later. The transfer function $\Gamma'(s)$ can be rewritten as

$$\Gamma'(s)=\frac{1+a_1 s+a_2 s^2}{(s+r_1)(s+r_2)(s+r_3)}. \tag{26}$$

The roots of (26) are

$$\begin{aligned} r_1&=-\frac{h_3}{3\sqrt[3]{2}b_3}+\frac{\sqrt[3]{2}h_2}{3b_3h_3}+\frac{b_2}{3b_3},\\ r_2&=\frac{(1-i\sqrt{3})h_3}{6\sqrt[3]{2}b_3}-\frac{(1+i\sqrt{3})h_2}{3\sqrt[3]{4}b_3h_3}+\frac{b_2}{3b_3},\\ r_3&=\frac{(1+i\sqrt{3})h_3}{6\sqrt[3]{2}b_3}-\frac{(1-i\sqrt{3})h_2}{3\sqrt[3]{4}b_3h_3}+\frac{b_2}{3b_3}, \end{aligned} \tag{27}$$

in which the following auxiliary variables have been defined as

$$\begin{aligned} h_1 &= 9b_1b_2b_3 - 2{b_2}^3 - 27{b_3}^2\,, \\ h_2 &= 3b_1b_3 - {b_2}^2\,, \\ h_3 &= \sqrt[3]{\sqrt{{h_1}^2 + 4{h_2}^3} + h_1}\,. \end{aligned} \tag{28}$$

To find the inverse Laplace transform (ILT) of $\Gamma'(s)$, it is rearranged as

$$\begin{aligned} \Gamma'(s) = \frac{1}{(s+r_1)(s+r_2)(s+r_3)} + a_1\frac{s}{(s+r_1)(s+r_2)(s+r_3)} \\ + a_2\frac{s^2}{(s+r_1)(s+r_2)(s+r_3)}\,. \end{aligned} \tag{29}$$

The ILT of the first term is [42]:

$$\begin{aligned} \mathscr{L}^{-1}\left\{\frac{1}{(s+r_1)(s+r_2)(s+r_3)}\right\} = \frac{e^{-r_1t}}{(r_1-r_2)(r_1-r_3)} \\ + \frac{e^{-r_2t}}{(r_1-r_2)(r_3-r_2)} + \frac{e^{-r_3t}}{(r_1-r_3)(r_2-r_3)}. \end{aligned} \tag{30}$$

Considering also the second and third terms (time derivatives of the first term), and reintroducing the term (-R), we obtain the ILT of $\Gamma(s)$:

$$\begin{aligned} \gamma(t) = -R\left[\frac{1 - r_1a_1 + {r_1}^2a_2}{(r_1-r_2)(r_1-r_3)}e^{-r_1t} + \frac{1 - r_2a_1 + {r_2}^2a_2}{(r_1-r_2)(r_3-r_2)}e^{-r_2t}\right. \\ \left. + \frac{1 - r_3a_1 + {r_3}^2a_2}{(r_1-r_3)(r_2-r_3)}e^{-r_3t}\right]\,. \end{aligned} \tag{31}$$

The final form can be generalised as

$$\gamma(t) = -R\cdot(k_1e^{-r_1t} + k_2e^{-r_2t} + k_3e^{-r_3t}). \tag{32}$$

B. Dynamic Regression Extension and Mixing

The DREM method constructs a linear regression based on (3). Assuming that p_{PFC} is known, the unknown parameters are H and p^*. Eq. (3) is repeated here in a rearranged form for convenience:

$$\dot{f} = \frac{1}{H}\left(\frac{1}{2}\frac{p_{PFC} - p_e}{f}\right) + \frac{p^*}{H}\left(\frac{1}{2f}\right). \tag{33}$$

The regression equation is constructed by applying a filter $\mathscr{F} = \alpha/(s+\alpha)$ to (3), where α>0 is a parameter of the filter. This filtering technique is employed to avoid a direct derivative action applied to f [43]. Defining the unknown parameters as

$$x_1 = \frac{1}{H};\; x_2 = \frac{p^*}{H}, \tag{34}$$

and the three filtered coefficients as

$$\begin{aligned} \xi_1 &= \mathscr{F}\left[\frac{1}{2}\frac{p_{PFC} - p_e}{f}\right] = \frac{\alpha}{s+\alpha}\left(\frac{1}{2}\frac{p_{PFC} - p_e}{f}\right); \\ \xi_2 &= \mathscr{F}\left[\frac{1}{2f}\right] = \frac{\alpha}{s+\alpha}\left(\frac{1}{2f}\right); \\ \xi_3 &= \mathscr{F}[\dot{f}] = \frac{\alpha s}{s+\alpha}(f), \end{aligned} \tag{35}$$

the regression takes the form

$$\xi_3 = x_1\cdot\xi_1 + x_2\cdot\xi_2. \tag{36}$$

1) Extension

As there are two unknown parameters but one equation, the regressor is extended by applying a dynamic operator $\mathscr{K}$ to (36). The delay operator is used because of its recognised efficiency in engineering applications [25]. It has the form:

$$[\mathscr{K}(\cdot)](t) = (\cdot)(t - t_d), \tag{37}$$

where t_d is the time delay. By combining the original regression and its extension, the matrix form is obtained:

$$\underbrace{\begin{bmatrix}\xi_3 \\ \xi'_3\end{bmatrix}}_{\mathbf{A}} = \underbrace{\begin{bmatrix}\xi_1 & \xi_2 \\ \xi'_1 & \xi'_2\end{bmatrix}}_{\mathbf{B}}\underbrace{\begin{bmatrix}x_1 \\ x_2\end{bmatrix}}_{\mathbf{x}}\,, \tag{38}$$

where $\xi'_{1,2,3}$ are the coefficients modified by $\mathscr{K}$.

2) Mixing

To decouple the regression, the mixing procedure consists of multiplying (38) by the adjoint (adj) of matrix $\mathbf{B}$. Since $adj(\mathbf{B})\cdot\mathbf{B} = \partial\cdot\mathbf{I}$, where ∂ is the determinant of $\mathbf{B}$ and $\mathbf{I}$ is the identity matrix, the regression takes its decoupled final form:

$$\mathbf{Z} = \partial\cdot\mathbf{x}, \tag{39}$$

where $\mathbf{Z}$ is defined as

$$\mathbf{Z} = adj(\mathbf{B})\cdot\mathbf{A}. \tag{40}$$

For a complete mathematical description of the DREM, the reader is referred to [25,44].

Data availability

Data will be made available on request.

References

[1] J.A.P. Lopes, C.L. Moreira, A.G. Madureira, Defining control strategies for microgrids islanded operation, IEEE Trans. Power Syst. 21 (2) (2006) 916–924.

[2] U. Tamrakar, D. Shrestha, M. Maharjan, B. Bhattarai, T. Hansen, R. Tonkoski, Virtual inertia: current trends and future directions, Appl. Sci. (2017).

[3] R. Ofir, U. Markovic, P. Aristidou, G. Hug, Droop vs. virtual inertia: comparison from the perspective of converter operation mode, IEEE Int. Energy Conf. (ENERGYCON) (2018).

[4] Q. Li, B. Ren, W. Tang, D. Wang, C. Wang, Z. Lv, Analyzing the inertia of power grid systems comprising diverse conventional and renewable energy sources, Energy Rep. 8 (2022) 15095–15105.

[5] B.K. Poolla, S. Bolognani, N. Li, F. Dörfler, A market mechanism for virtual inertia, IEEE Trans. Smart Grid 11 (4) (2020) 3570–3579.

[6] E. Heylen, F. Teng, G. Strbac, Challenges and opportunities of inertia estimation and forecasting in low-inertia power systems, Renew. Sustain. Energy Rev. 147 (2021) 111176.

[7] A. García, Á. Ortega, L. Rouco, and L. Sigrist, A review of methods for the estimation of inertia and its distribution. Institute for Research in Technology, Comillas Pontifical University, Madrid, 2021.

[8] B. Tan, J. Zhao, M. Netto, V. Krishnan, V. Terzija, Y. Zhang, Power system inertia estimation: review of methods and the impacts of converter-interfaced generations, Int. J. Electr. Power Energy Syst. 134 (2022) 107362.

[9] S.C. Dimoulias, E.O. Kontis, G.K. Papagiannis, Inertia estimation of synchronous devices: review of available techniques and comparative assessment of conventional measurement-based approaches, Energies (Basel) 15 (20) (2022).

[10] K. Prabhakar, S.K. Jain, P.K. Padhy, Inertia estimation in modern power system: a comprehensive review, Electr. Power Syst. Res. 211 (2022) 108222.

[11] E. Ørum, M. Kuivaniemi, M. Laasonen, A.I. Bruseth, E.A. Jansson, A. Danell, K. Elkington, and N. Modig, Future system inertia. ENTSO-e, Bruxelles, Belgium, 2018.

[12] P. Du, J. Matevosyan, Forecast system inertia condition and its impact to integrate more renewables, IEEE Trans. Smart Grid 9 (2) (2018) 1531–1533.

[13] P.K. Dhara, Z.H. Rather, Non-synchronous inertia estimation in a renewable energy integrated power system with reduced number of monitoring nodes, IEEE Trans. Sustain Energy 14 (2) (2023) 864–875.

[14] D. Zografos, M. Ghandhari, R. Eriksson, Power system inertia estimation: utilization of frequency and voltage response after a disturbance, Electr. Power Syst. Res. 161 (2018) 52–60.

[15] G. Cai, B. Wang, D. Yang, Z. Sun, L. Wang, Inertia estimation based on observed electromechanical oscillation response for power systems, IEEE Trans. Power Syst. 34 (6) (2019) 4291–4299.

[16] B. Tan, J. Zhao, Data-driven time-varying inertia estimation of inverter-based resources, IEEE Trans. Power Syst. 38 (2) (2023) 1795–1798.

[17] R.K. Panda, A. Mohapatra, S.C. Srivastava, Online estimation of system inertia in a power network utilizing synchrophasor measurements, IEEE Trans. Power Syst. 35 (4) (2020) 3122–3132.

[18] M. Liu, J. Chen, F. Milano, On-line inertia estimation for synchronous and non-synchronous devices, IEEE Trans. Power Syst. 36 (3) (2021) 2693–2701.

[19] B. Tan, J. Zhao, V. Terzija, Y. Zhang, Decentralized data-driven estimation of generator rotor speed and inertia constant based on adaptive unscented Kalman filter, Int. J. Electr. Power Energy Syst. 137 (2022) 107853.

[20] J. Guo, X. Wang, B.-T. Ooi, Estimation of inertia for synchronous and non-synchronous generators based on ambient measurements, IEEE Trans. Power Syst. 37 (5) (2022) 3747–3757.

[21] M. Mazidi, T. McKelvey, P. Chen, A pure data-driven method for online inertia estimation in power systems using local rational model approach, IEEE Trans. Ind. Appl. 59 (5) (2023) 5506–5516.

[22] F. Zeng, J. Zhang, G. Chen, Z. Wu, S. Huang, Y. Liang, Online estimation of power system inertia constant under normal operating conditions, IEEE Access 8 (2020) 101426–101436.

[23] K. Tuttelberg, J. Kilter, D. Wilson, K. Uhlen, Estimation of power system inertia from ambient wide area measurements, IEEE Trans. Power Syst. 33 (6) (2018) 7249–7257.

[24] T. Kerdphol, M. Watanabe, R. Nishikawa, Y. Hayashi, Y. Mitani, Inertia estimation of the 60 Hz Japanese power system from synchrophasor measurements, IEEE Trans. Power Syst. 38 (1) (2023) 753–766.

[25] J. Schiffer, P. Aristidou, R. Ortega, Online estimation of power system inertia using dynamic regressor extension and mixing, IEEE Trans. Power Syst. 34 (6) (2019) 4993–5001.

[26] W. Zhang, Y. Wen, C.Y. Chung, Impedance-based online estimation of nodal inertia and primary frequency regulation capability, IEEE Trans. Power Syst. (2022) 1–12.

[27] J. Zhang, H. Xu, Online identification of power system equivalent inertia constant, IEEE Trans. Ind. Electron. 64 (10) (2017) 8098–8107.

[28] E.M. Carlini, F. Del Pizzo, G.M. Giannuzzi, D. Lauria, F. Mottola, C. Pisani, Online analysis and prediction of the inertia in power systems with renewable power generation based on a minimum variance harmonic finite impulse response filter, Int. J. Electr. Power Energy Syst. 131 (2021) 107042.

[29] F. Allella, E. Chiodo, G.M. Giannuzzi, D. Lauria, F. Mottola, On-line estimation assessment of power systems inertia with high penetration of renewable generation, IEEE Access 8 (2020) 62689–62697.

[30] E.S.N.R. Paidi, H. Marzooghi, J. Yu, V. Terzija, Development and validation of artificial neural network-based tools for forecasting of power system inertia with wind farms penetration, IEEE Syst. J. 14 (4) (2020) 4978–4989.

[31] J.D. Rios Penaloza, A. Prevedi, A. Joshi, F. Napolitano, F. Tossani, A. Borghetti, On-line inertia estimation in presence of distributed energy resources, 6th International Conference on Smart Energy Systems and Technologies (SEST) (2023).

[32] J. Machowski, Z. Lubosny, J. Bialek, J.R. Bumby, Power System Dynamics, Stability and Control, Third Ed., John Wiley & Sons Ltd, Croydon, UK, 2020.

[33] P.M. Anderson, M. Mirheydar, A low-order system frequency response model, IEEE Trans. Power Syst. 5 (3) (1990) 720–729.

[34] E.O. Kontis, I.D. Pasiopoulou, D.A. Kirykos, T.A. Papadopoulos, G.K. Papagiannis, Estimation of power system inertia: a comparative assessment of measurement-based techniques, Electr. Power Syst. Res. 196 (2021) 107250.

[35] R. Ortega, V. Nikiforov, D. Gerasimov, On modified parameter estimators for identification and adaptive control. A unified framework and some new schemes, Annu. Rev. Control 50 (2020) 278–293.

[36] L. Gérin-Lajoie, Report on the EMTP-RV 39-bus system, 2015.

[37] S. D'Arco, J.A. Suul, Virtual synchronous machines - classification of implementations and analysis of equivalence to droop controllers for microgrids, 2013 IEEE Grenoble Conference PowerTech, POWERTECH 2013 (2013).

[38] F. Milano, F. Dorfler, G. Hug, D.J. Hill, G. Verbic, Foundations and challenges of low-inertia systems (Invited Paper), 2018 Power Systems Computation Conference (PSCC) (2018) 1–25.

[39] F. Mandrile, V. Mallemaci, E. Carpaneto, R. Bojoi, Lead-lag filter-based damping of virtual synchronous machines, IEEE Trans. Ind. Appl. 59 (6) (2023) 6900–6913.

[40] R. Ofir, U. Markovic, P. Aristidou, G. Hug, Droop vs. virtual inertia: comparison from the perspective of converter operation mode, 2018 IEEE International Energy Conference (ENERGYCON) (2018) 1–6.

[41] G. Han, L. Xiong, L. You, Z. Ling, M. Liu, Y. Cui, S. Zhang, Z. Fang, A simple estimation method of grid-forming inverter inertia based on rate of change of frequency, IET Power Electron. 17 (5) (2024) 591–602.

[42] Anatolij Platonovič Prudnikov, Urij Aleksandrovič Bryčkov, Oleg Igorevich Marichev. Integrals and Series, Volume 5: Inverse Laplace Transforms, 1st. Edition, CRC Press, 1992.

[43] P.A. Ioannou, J. Sun. Robust Adaptive Control, Prentice Hall, 1995.

[44] S. Aranovskiy, A. Bobtsov, R. Ortega, A. Pyrkin, Performance enhancement of parameter estimators via dynamic regressor extension and mixing, IEEE Trans. Autom. Contr. 62 (7) (2017) 3546–3550.